IEEE Access
Multidisciplinary ⋮ Rapid Review ⋮ Open Access Journal

Received 1 November 2023, accepted 18 November 2023, date of publication 23 November 2023,
date of current version 29 November 2023.

Digital Object Identifier 10.1109/ACCESS.2023.3335938

RESEARCH ARTICLE

Propagation Characteristics of Extremely Low-Frequency Electromagnetic Waves in a Uniformly Infinite Polar "Sea-Sea Ice" Half-Space

SUMOU HU[1], HUI XIE[1], AND JIANCHEN FENG[2]
[1]College of Electronic Engineering, Naval University of Engineering, Wuhan 430033, China
[2]Unit 91388 of the People's Liberation Army, Zhanjiang 524000, China

Corresponding author: Hui Xie (0909031059@nue.edu.cn)

ABSTRACT In this study, we accurately calculated the propagation characteristics of extremely low-frequency (ELF) electromagnetic waves (EMWs) excited by horizontal electric dipoles (HEDs) in the uniformly infinite polar "sea-sea ice" half-space. This was achieved by combining the program platform written by the message passing interface (MPI) with the three-dimensional total field scattered field source finite difference time domain (TSS-FDTD) method to develop an improved calculation method of parallel TSS-FDTD electromagnetic field. Using equivalent principle and boundary grid field value transformation technology, the calculation space of electromagnetic field (EMF) in seawater and sea ice is divided into several regional grids to establish the calculation model of TSS-FDTD in the polar "sea-sea ice" half-space. The maximum radiation direction and average minimum attenuation of ELF EMF in the uniformly infinite polar "sea-sea ice" half-space (near the interface between seawater and sea ice) are obtained. The simulation results show that, at depth $d = 10$ m and propagation distance $\rho = 125$ m from the interface between seawater and sea ice, the maximum radiation directions of EMF intensity are vertical electric field direction E_z and horizontal magnetic field direction H_x, respectively; moreover, their average minimum attenuation values in the sea water medium are 30 dB and 20 dB, respectively, and their corresponding values in sea ice medium are 20 dB and 10 dB, respectively. Therefore, compared with the directions of other electric and magnetic field components, these directions more suitable for receiving underwater signals. Finally, we selected different thickness values of the sea ice medium for simulation, and compared the results with the Sommerfeld numerical integration method (SNIM) proposed by Pan. The results show that the calculation results of the two methods are consistent, and that the average error is less than 5%, which verifies the effectiveness and accuracy of the proposed method.

INDEX TERMS Extremely low-frequency (ELF), electromagnetic waves, horizontal electric dipole (HED), sea, finite difference time domain (FDTD).

I. INTRODUCTION

With the development in ocean resource extraction technologies and the deepening of ocean exploration, the exploitation and utilization of polar marine resources has gained strategic significance for all countries. However, due to the cold climate, harsh natural environment and year-round ice and snow, the exploration of the polar ocean has always been a challenging task. Among the existing marine exploration technologies, that based on extremely low-frequency (ELF) electromagnetic waves (EMWs) is relatively mature and has been widely used in many engineering fields including underwater communication, underwater navigation, and seabed exploration [1], [2], [3]. However, limited by the detection ability of traditional ELF EMW-based detection systems and the heavy influence of complex factors such as weather, geomagnetic field, and ionospheric disturbance in the polar region, few achievements have been made

The associate editor coordinating the review of this manuscript and approving it for publication was Yougan Chen.

in the field of resource detection in polar ocean. Among many computational methods used for solving problems on underwater propagation of EMWs, Sommerfeld numerical integration method (SNIM) is the most theoretically mature approach [4]. However, due to the existence of discrete singular points in the complex plane, obtaining a highly precise numerical solution becomes cumbersome. In the following decades, scholars simplified the Sommerfeld integral method to varying degrees to obtain the propagation characteristics of EMWs in different media [5], [6], [7], [8], [9], but the process of solving it mathematically is highly complex., which makes it very difficult to apply in studies on ocean exploration.

Recently, with the advancements in computational electromagnetics, the finite difference time domain (FDTD) method has been established as an effective tool for calculations related to low-frequency EMWs, because of its intuitive physical process and simple calculation format. The first proposal to use FDTD numerical method for solving problems on low-frequency EMWs was in a conference article published by Berenger [10] in 1994. In the following years, Berenger further improved the FDTD numerical method and proposed various methods to increase the efficiency of simulation calculation [11], [12], but his research mainly focused on the propagation of low-frequency EMWs in the earth-ionosphere space model. Xia and Sullivan [13] successfully employed the FDTD method to calculate the propagation characteristics of underwater ELF EMWs. The FDTD method was applied in combination with the method of two equations and two unknowns (2E2U) [14] to obtain the propagation characteristics of EMWs in lake water. However, because Sullivan's research is focused on the propagation of EMWs in lake environment, which is not applicable to their propagation in seawater environment. Zheng et al. [15] was the first to propose a new three-dimensional (3D) total field scattered field source (TSS) FDTD method based on the equivalence principle, which is suitable for simulating low-frequency EMWs in vast ocean with complex and fine targets; this approach has yielded some valuable results. In the same year, Zheng et al. also proposed a new parallel TSS-FDTD method [16]. This method was adopted by Yang et al. [17], who combined it with the sea-air boundary field value conversion and the thin line algorithm to specifically analyze the field distribution near the very low-frequency (VLF) antenna array in seawater. This method includes three FDTD calculations: The first calculation is used to obtain the fields in the area with fine meshes, such as the area near the excited source. The second is to calculate the fields in the area with coarse meshes, such as extensive background space. In this step, if the required computational resources are high or the computation space is vast, some part of the second FDTD calculation can be performed as the third FDTD calculation. The relationship between each calculation is established by setting a TSS boundary. The TSS-FDTD method inherits the advantages of the conventional FDTD method, and is suitable for analyzing low-frequency EMW propagation in lossy media, such as seawater. However, although the TSS-FDTD method can solve the above calculation problem, considerable running time is required to deal with the field distribution in a wide computing space because each step calculation is still FDTD calculation. Thus, it cannot be directly and effectively applied to the EMW propagation in polar seawater space environment.

Based on the program platform written using message passing interface (MPI), in this study, we employed the equivalent principle and boundary grid field value transformation technology to partition the calculation area of EMF strength in the polar ''sea-sea ice'' half-space to propose an improved parallel TSS FDTD method. The distribution of the ELF field excited by the horizontal electric dipoles (HEDs) in the half-space of the polar ''sea-sea ice'' is calculated. The method presented in this paper can be divided into three independent calculations introduced in in Section II. The first step of TSS-FDTD calculation is the traditional FDTD calculation, which yields the near-field EMF intensity of the ELF field source. The second step of TSS-FDTD calculation uses the equivalence principle and the boundary grid field value transformation technology to calculate the EMF intensity in the scattering field space. Based on the results of the second calculation, the third step of TSS-FDTD calculation is performed by using the same approach to calculate the EMF amplitude in the whole polar ''sea-sea ice'' half-space. It is worth noting that the equivalent transformation principle and boundary grid field value transformation proposed in this paper can be used for regional block processing of EMFs in layered media, and the calculation results are more rapid and efficient. In Section III. A, we use the proposed method to simulate and analyze the characteristics of ELF EMW field intensity distribution in the polar ''sea-sea ice'' half-space, and get the maximum field intensity radiation direction and the average minimum attenuation value. In Section III-B, we selected sea ice medium layers of different thicknesses and compared the numerical calculation results with those of SNIM proposed by Pan [18] to verify the accuracy of our proposed method.

II. IMPLEMENTATION OF THE IMPROVED PARALLEL TSS-FDTD METHOD

A. PARALLEL TSS-FDTD CALCULATION MODEL

The FDTD method is a numerical method used for studying time-domain full-wave EMFs by solving differential Maxwell equations [19], [20], [21]. The electric field $\boldsymbol{E}$ and magnetic field $\boldsymbol{H}$ components of this method adopt the discrete mode of alternating sampling in space and time. In other words, each $\boldsymbol{E}$ (or $\boldsymbol{H}$) field component is surrounded by four $\boldsymbol{H}$ (or $\boldsymbol{E}$) field components. The Maxwell curl equation with time variable is transformed into a set of difference equations using this discrete method, and the space EMF is solved stepwise on the time axis.

TSS-FDTD method includes three independent FDTD calculation processes, as shown in Fig. 1. Fig. 1(a) shows the near-field calculation space used in the first step of TSS-FDTD calculation, Fig. 1(b) shows the scattering field calculation space considered in the second step of TSS-FDTD calculation, and Fig. 1(c) shows the full calculation space used in the third step of TSS-FDTD calculation. In the first step of TSS-FDTD calculation, the near-field space is divided using a fine mesh, whereas the scattered field and the whole space are divided using a cluster mesh to obtain the field distribution in the near-field space. In the second step of TSS-FDTD calculation, the field distribution of the scattering field space is obtained based on the equivalence principle and the results of the first calculation. Finally, all the field values needed for the third step of TSS-FDTD calculation on the output boundary are added as the TSS at the boundary to realize the grid transformation. Then, the field distribution of the whole space is calculated. The cubic FDTD calculation uses the TSS transformation boundary as a bridge, as shown in Fig. 1. Because the electric and magnetic fields in FDTD are alternately sampled and discrete, the transform boundary consists of two electric field boundaries ($\boldsymbol{E}$ surface) and magnetic field boundaries ($\boldsymbol{H}$ surface) adjacent to each other. In this study, the convolutional perfect matching layer (CPML) [22] was used as the absorption boundary.

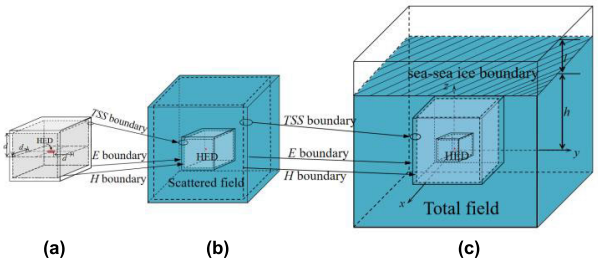

FIGURE 1. TSS-FDTD calculation model in polar seawater space. (a) The near-field space considered in the first calculation; (b) the scattering field space used in the second calculation; (c) full space considered in the third calculation.

B. EQUIVALENCE PRINCIPLE TECHNIQUE

The Huygens equivalence principle [23] is used to calculate the EMF of the total field and the scattered field by extrapolating from the near field source. Fig. 2 shows the equivalent schematic diagram of TSS-FDTD calculation.

In the first step of TSS-FDTD calculation, the transform boundary surrounding the excitation current source $\boldsymbol{J}_s$ and magnetic current source $\boldsymbol{J}_{ms}$ is established, and the EMF on the transform boundary is recorded as a distribution of its $\boldsymbol{E}$ and $\boldsymbol{H}$ components. The corresponding electromagnetic current can be expressed as:

$$\begin{cases} \boldsymbol{J}_s = \boldsymbol{e}_n \times \boldsymbol{H} \\ \boldsymbol{J}_{ms} = -\boldsymbol{e}_n \times \boldsymbol{E} \end{cases} \tag{1}$$

where, $\boldsymbol{e}_n$ represents the outer normal unit vector of the transformation surface. The second and third step of TSS-FDTD calculations are based on the electric field boundary. The region within the electric field boundary is the scattering field region, whereas the region outside it is the total field region. Based on the equivalence principle and the total field scattering technique, the surface electromagnetic flow obtained from the first step of TSS-FDTD calculation is used to complete the process of adding the incident plane wave at the transform boundary in the second step of TSS-FDTD calculation. Finally, in the third step of TSS-FDTD calculation, the EMF distribution in the whole space is calculated again by using same techniques.

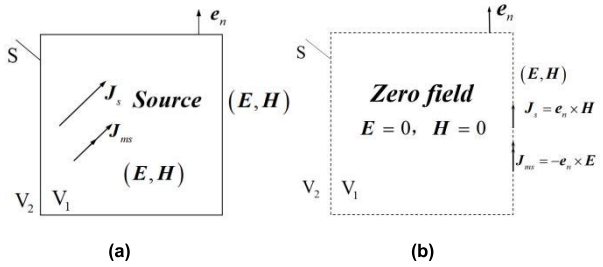

FIGURE 2. The equivalent principle of TSS-FDTD calculation. (a) The original problem; (b) equivalence problem.

C. BOUNDARY GRID FIELD VALUE TRANSFORMATION ALGORITHM

This method is further illustrated by taking the boundary grid field value transformation technology of the total field-scattering field in the case of transverse magnetic (TM) waves as an example. We define (E, H) and (E', H') as the EMF nodes of the first and second step of TSS-FDTD calculations, respectively. We denoted the space discrete distance values in the first and second step of TSS-FDTD calculations as δ_1 and δ_2, respectively, and the value of grid transformation multiple (N) was considered to be δ_2/δ_1. First, the range of the boundary between the total field and the scattering field used in the second step of TSS-FDTD calculation was determined. Here, the boundary of the total field is defined as the boundary of the electric field with range $\left\{i'_0\delta_2 \le x \le i'_a\delta_2, j'_0\delta_2 \le y \le j'_b\delta_2\right\}$. Furthermore, the boundary corresponding to the range of electric field considered in the first step of TSS-FDTD calculation was expressed as $\{i_0\delta_1 \le x \le i_a\delta_1, j_0\delta_1 \le y \le j_b\delta_1\}$. In other words, in the second step of TSS-FDTD calculation, there are $i'_a - i'_0 + 1, j'_b - j'_0 + 1$ E'_z nodes on the edges located on x and y axes, respectively. Correspondingly, there are $N_{(i'_a - i'_0)} + 1$, $N_{(j'_b - j'_0)} + 1$ E'_z nodes on the edge considered in the first step of TSS-FDTD calculation. For different values of N, the distribution of the EMF nodes on the boundary of the total field-scattering field varies considerably. Fig. 3(a) and (b) show the distribution of EMF nodes in two calculations on the $-x$ boundary for the grid transformation ratios of odd and even times, respectively. Where the field quantities in the first step of TSS-FDTD calculation are denoted without "′", and those in the second step of TSS-FDTD calculation are denoted with "′".

Consider the equivalent electromagnetic flow on the boundary $x = i_0'\delta_2$ as expressed in Eq. (1). According to Maxwell curl equations

$$\begin{cases} \nabla \times \boldsymbol{H}' = \dfrac{\partial \boldsymbol{D}'}{\partial t} + \boldsymbol{J}' + \boldsymbol{J}_s \\ \nabla \times \boldsymbol{E}' = -\dfrac{\partial \boldsymbol{B}'}{\partial t} - \boldsymbol{J}'_m - \boldsymbol{J}_{ms} \end{cases} \tag{2}$$

Considering the surface of normal $\boldsymbol{e}_n = -\boldsymbol{x}$, the equivalent electromagnetic currents are

$$\begin{cases} \boldsymbol{J}_s = \boldsymbol{e}_n \times \boldsymbol{H} = -\boldsymbol{x} \times (H_x, H_y, 0) = -H_y \boldsymbol{z} \\ \boldsymbol{J}_{ms} = -\boldsymbol{e}_n \times \boldsymbol{E} = \boldsymbol{x} \times (0, 0, E_z) = -E_z \boldsymbol{y} \end{cases} \tag{3}$$

By substituting Eq. (3) into Eq. (2), the component equation is obtained as

$$\begin{cases} \dfrac{\partial H'_y}{\partial x} - \dfrac{\partial H'_x}{\partial y} = \varepsilon \dfrac{\partial E'_z}{\partial t} - H_y \boldsymbol{z} \\ -\dfrac{\partial E'_z}{\partial x} = -\mu \dfrac{\partial H'_y}{\partial t} + E_z \boldsymbol{y} \end{cases} \tag{4}$$

Thus, the difference discretization of Eq. (4) in time and space can be used to obtain the iterative formula in the form of FDTD input on the boundary of TSS.

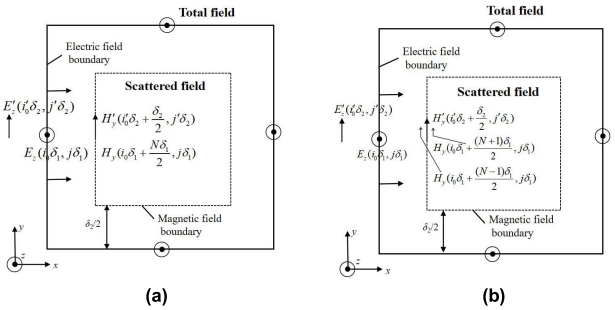

FIGURE 3. Node distribution on the boundary of the total field scattering field in TM mode. (a) when *N* is an odd number; (b) when *N* is even.

D. SUBDOMAIN CALCULATION

In order to enhance the computational efficiency of 3D parallel TSS-FDTD, we integrated the parallel program, developed using Fortran90 language with MPI functions [24], into the TSS-FDTD method. This allowed us to divide the entire computation region of TSS-FDTD into multiple subdomains, as depicted in Fig. 4. In this approach, the calculation area is partitioned into several subdomains. During the iterative process, each process independently computes one of the subdomains. Although the calculation procedures remain the same, the processed data vary. Prior to iterating the electric field (magnetic field) within a subdomain, the internal field quantity is iterated according to the conventional FDTD. The computation of the boundary electric field (or magnetic field) component necessitates the value of the magnetic field (electric field) component corresponding to the first half time of the neighboring subdomain. Consequently, it is essential to transfer the electromagnetic constants at the interface between each process and ensure the synchronization of the iterative calculation of the electromagnetic field quantity in each subdomain. This ensures that the field value solution of the FDTD method, specifically the iterative formula of the total field scattering field source, can be accomplished, thereby realizing the optimized parallel algorithm. Fig. 4 relates to the initialization functions that the MPI system must call: Call MPI_Init ();

Call MPI_Comm_Rank ();

Call MPI_Comm_Size ();

Call MPI_Finalize

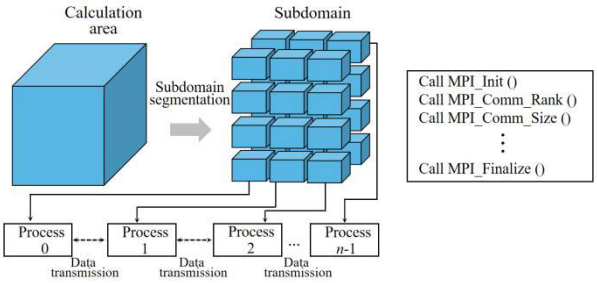

FIGURE 4. Parallel TSS-FDTD calculation method based on MPI platform.

The MPI_Init () and MPI_Finalize () functions serve as a pair of instructions to initiate and terminate an MPI system. The MPI_Comm_Rank () function retrieves the process's sequence number in the communication. The MPI_Comm_Size () function retrieves the number of processes called. This article employs version MPICH2-1.2.1.

This method achieves simultaneous computation of multiple subdomain tasks through parallel computation, parallelizing the original serial computation. This significantly enhances the computational efficiency and reduces the computation time. Each process calculates one or more subdomains, and the field value of the TSS-FDTD method can be solved by exchanging the electromagnetic field at the interface between each process. Fig. 4 illustrates the calculation model diagram of TSS-FDTD based on the MPI parallel program.

III. NUMERICAL RESULTS OF ELECTRIC DIPOLES

In this section, two cases are discussed in detail: (1) Radiation field propagated by ELF EMWs excited by HEDs in polar "sea-sea ice" half-space. (2) Calculation and verification of the proposed method.

A. FIELD DISTRIBUTION IN SEAWATER AND SEA ICE SPACE

To obtain the field propagation characteristics in the two-layer medium of seawater and sea ice, as shown in Fig. 1, we adopted the calculation model of parallel TSS-FDTD method for polar seawater space.

HED with an operating frequency of 10 Hz was placed in the xoy plane with the origin located in the water $h = 10$ m from the sea ice. Moreover, an independent voltage source

was placed at the center point of the antenna. The radius of the HED source is 2 cm. Based on their EMW propagation characteristics, we generally consider the conductivity of seawater to be $\sigma_{sea} = 4$ S/m, and that of sea ice as $\sigma_{ice} = 3.2$ S/m [18]. Because the seawater and sea ice media are high consumption media, their permittivity is complex and can be expressed as $\varepsilon = \varepsilon_r + j\sigma/\omega = \beta + j\alpha$, where $\varepsilon_r \approx 80$ F/m denotes the relative dielectric constant, which signifies the relative capacity of the dielectric material to retain electrostatic energy within the electric field. $\beta = \alpha = (\omega\mu_0\sigma/2)^{1/2} = (\pi\mu_0\sigma f)^{1/2}$, where, ω denotes the angular frequency. The permeability is $\mu_0 = 4\pi\times10^{-7}$H/m, the wave number of EMW propagation is $k = \omega(\mu_0\varepsilon)^{1/2}$, and the wavelength is $\lambda = 2\pi/\beta$. The calculated value of the wavelength of a 10 Hz EMW is approximately 500 m in seawater and approximately 559 m in sea ice. The calculation parameters of seawater and sea ice media are listed in Table 1.

TABLE 1. Calculation parameters of seawater and sea ice media.

Materials	Electric conductivity σ (S/m)	Dielectric constant ε (F/m)	Magnetic permeability μ (H/m)
Sea	4	80	$4\pi\times10^{-7}$
Sea ice	3.2	80	$4\pi\times10^{-7}$

Due to the fine structure of the wired antenna, the calculation of TSS-FDTD in this case is performed in three steps. In the first step, the calculation space is a dark shadow region cube divided by a fine grid, set to 20 m × 30 m × 20 m, and its spatial discrete interval is set to $\delta_1 = 0.1$ m. This step yields the field of the region around the excitation source. The calculation space in the second step is the scattering field model area, which is divided by coarse mesh. This area is set as 100 m × 130 m × 100 m, and the spatial discrete interval is $\delta_2 = 0.5$ m; thus, $N = \delta_2/\delta_1 = 5$. In the third step, the entire calculation space, divided by coarse mesh, is set to 1000 m × 1500 m × 1000 m. The spatial discrete interval in this case is $\delta_3 = 2.5$ m; thus, $N = \delta_3/\delta_2 = 5$. The depth h in this calculation is set to 10 m. The second and third calculation regions are shown in Fig. 1. The magnetic fields of the these two regions were calculated using the equivalent electromagnetic currents obtained from the first calculation. Finally, the field of the entire computing space, including seawater and sea ice, was calculated using an AMD Ryzen Threadripper 3990X 64-core processor 2.90 GHz workbench. The memory consumption time was approximately 1.15 hours, and the amount of memory consumed was 365.7 MB. These performance metrics were compared with those of the conventional TSS-FDTD method, and the consumption table is provided in Table 2. The calculation time of the proposed method is 32.6% of that of conventional TSS-FDTD method and the memory consumption is 32.9% of conventional TSS-FDTD method. This demonstrates the superiority of the proposed method.

TABLE 2. The calculated parameters, consumed memory, and required time for the conventional and proposed algorithms.

Algorithm		Spatial discrete interval σ (m)	Program run time t (s)	Memory consumption (MB)	Computing space (m×m×m)
Conventional TSS-FDTD algorithm (N=5)	First calculation	0.5	4156	415.3	120×160×120
	Second calculation	2.5	7094	693.4	1000×1500×1000
Parallel TSS-FDTD algorithm (N=5)	First calculation	0.1	623	53.3	20×30×20
	Second calculation	0.5	770	81.6	100×130×100
	Third calculation	2.5	2280	229.8	1000×1500×1000

On the premise of maintaining generality, an independent voltage source was placed at the center point of the HED to excite the HED source. According to the above EMF calculation formula, the wavelength of 10 Hz EMW in seawater is approximately 500 m. The conductivity values of seawater and sea ice in a uniformly infinite space is $\sigma_{sea} = 4$ S/m and $\sigma_{ice} = 3.2$ S/m, respectively, and the relative dielectric constant of seawater and sea ice is $\varepsilon \approx 80$ F/m. The observation point and the source point were located on the same horizontal plane 10 m away from the sea-sea ice interface. The CPML condition was applied to the absorption boundary condition to truncate the outward-propagating EMW. This method yielded the variation in the EMF components of the electric dipole in the seawater and sea ice dielectric in addition to the propagation distance. In the model shown in Fig. 1, with the dipole source as the center, square regions with length and width of 300 m were selected on the xoy plane of the horizontal section, yoz of the vertical section, and xoz plane. Moreover, a combined simulation and calculation using MATLAB and the EastFDTD software from Dongjun Technology Company was conducted to generate the amplitude distribution diagram of the magnetic field components in the three regions. The diagram is presented in Fig. 5.

Fig. 5 plots the variation in the attenuation of EMWs on both sides of the interface. The upper half of the space represents the change in EMW propagation in sea ice medium, while the lower half represents that in the sea water medium. As shown, the propagation speed of ELF EMW in seawater is slower than that in sea ice. This is because the electrical conductivity in sea water is greater than that in sea ice, and the attenuation speed of EMW in sea water is faster than that in the sea ice. Furthermore, Fig. 5 clearly shows that the radiation field intensity of the EMF at the interface between seawater and sea ice undergoes an obvious sudden change. Figs. 5(a)-(c) clearly show that, compared with the electric field intensities in the E_x and E_y directions, that in the E_z direction is the strongest. Moreover, the average attenuation value in seawater is approximately 30 dB at 125 m from the electric dipole source, and that in sea ice is approximately 20 dB. The electric field intensity in E_y direction is stronger than that in the E_x direction, which is the weakest. At 125 m from the dipole source and in the direction of the electromagnetic component E_x, the approximately values of average attenuation in seawater and sea ice are 60 dB and 40 dB, respectively. Figs. 5(d)-(f) show

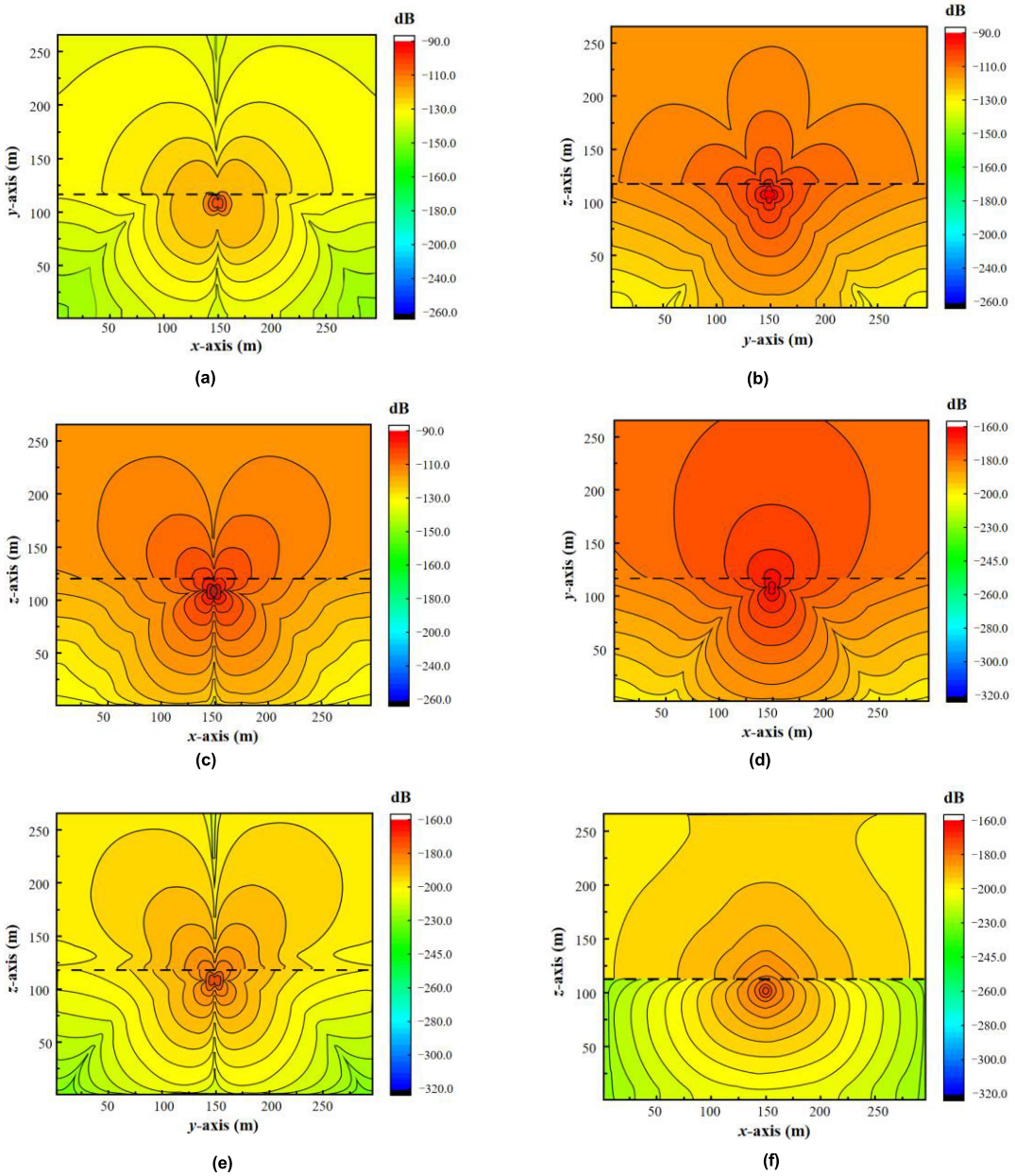

FIGURE 5. HED on the xoy plane in polar seawater environment, operating frequency $f = 10$ Hz, and variation in EMF amplitude variation in the vicinity of ELF source underwater $h = 10$ m. (a) E_x; (b) E_y; (c) E_z; (d) H_x; (e) H_y; (f) H_z.

that, compared with the magnetic field intensity in H_y and H_z directions, that in the H_x direction is the strongest. At 125 m from the dipole source, the approximate values of average attenuation in seawater and sea ice are 20 dB and 10 dB, respectively. At the same distance from the dipole source, in the direction of the minimum magnetic field component H_z, the approximate values of average attenuation in seawater and sea ice are 65 dB and 40 dB, respectively. According to the EMW propagation principle [25], the attenuation rate of ELF in seawater is approximately $0.1 \sim 0.5$ dB/m, which is roughly consistent with the numerical simulation results of the proposed method, thus proving its accuracy. The results show that the electric field direction E_z and magnetic field direction H_x are suitable for long-distance propagation in xoy plane in polar seawater. This finding is applicable for target tracking and detection in polar seawater.

B. COMPARISON AND VERIFICATION

To verify the effectiveness of the proposed method, an example has been provided. The results obtained using the proposed method are compared those obtained using Pan's approximation SNIM [18]. The entire calculation model is shown in Fig. 1. To elaborate, a y-polarized electric dipole with an amplitude of 1 A·m and operating frequency $f = 10$ kHz is placed below the sea surface. The distance h

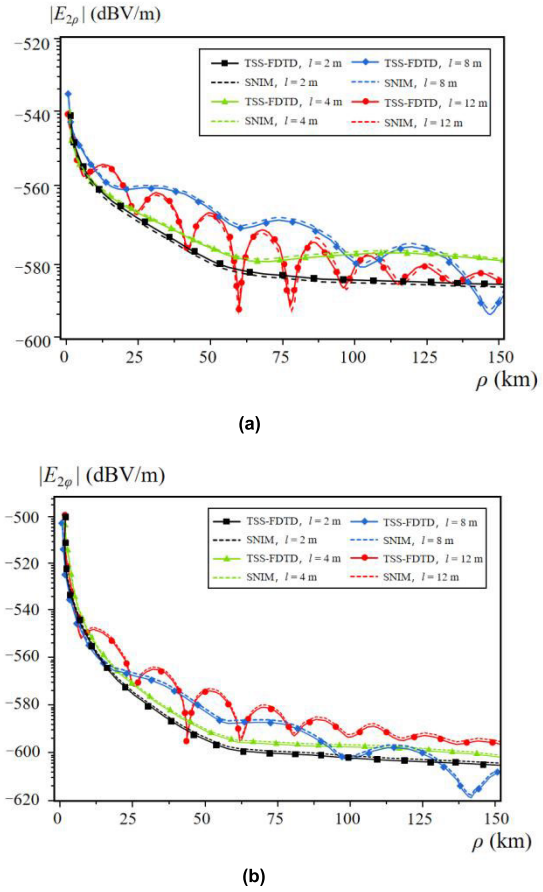

FIGURE 6. Comparison of the electric field components obtained using the proposed method with those obtained using Pan's SNIM method for different ice thickness values in polar environment. (a) $E_{2\rho}$; (b) $E_{2\varphi}$.

between the excitation source and the sea surface was set to 10 m. The electric parameters k, μ, ε, σ in seawater and sea ice media remain unchanged, and the wavelengths of EMW with $f = 10$ kHz in lossless seawater and sea ice media are 16 m and 18 m, respectively. Furthermore, the observation point and the excitation source are located at the same level, and the system origin is set at the center of the electric dipole antenna.

To simplify the calculation of TSS-FDTD method, it was divided into three steps. In the first step, the field around the excited dipole source was obtained considering the element size of TSS-FDTD to be 0.1 m. The calculation area for the first calculation is shown in Fig. 1(a). The output boundary consists of an $\boldsymbol{E}$ boundary and an $\boldsymbol{H}$ boundary. To facilitate a more accurate calculation when using the FDTD technique, the new values of each EMF component $\boldsymbol{E}$ and $\boldsymbol{H}$ of each grid point in Fig. 1 (a) are separated by 1/2 Yee cell from the neighboring field components. The distance from the output boundary to the end of the dipole is denoted by d, and based on the wavelength obtained at 10 kHz in seawater, we set the calculation area of the near-field region considered in the first calculation to 40 units, which is approximately 4 m. In the second step, the equivalent electromagnetic currents recorded in the first step are used to obtain the fields in other sea areas. In the third step, we derive the field in the sea ice from the equivalent EMF at the sea surface. The current is also obtained from the output boundary in the first calculation. To validate the proposed method and verify its accuracy, we plotted its results for comparison with those obtained using the Pan's SNIM, as shown in Fig. 6.

Fig. 6 shows the variation curves of field intensities of $E_{2\rho}$ and $E_{2\varphi}$ (subscript 2 represents seawater medium) in the direction of $\varphi = 0°$ with the propagation distance when the ice thickness values are 2 m, 4 m, 8 m, and 12 m. As shown, the results of the two methods agree well. For propagation distance ρ values less than 25 km, the amplitude of the electric field components $E_{2\rho}$ and $E_{2\varphi}$ decays the fastest. For $\rho > 25$ km, the amplitude attenuation of the electric field component $E_{2\rho}$ and $E_{2\varphi}$ changes to different degrees. The higher the thickness of sea ice dielectric layer l, the greater the fluctuation in the amplitude of the electric field component; however, as mentioned earlier, the change curves remain consistent for both methods. Moreover, as shown, the errors of both methods tend to increase with the increase of the propagation distance ρ. The maximum error value is less than 3 dB and the average relative error is less than 5% in the ELF band. These error values satisfy the engineering requirement, and verifies the accuracy and effectiveness of the proposed method.

IV. CONCLUSION

In this paper, we propose an improved parallel TSS-FDTD method based on MPI programming platform. It uses region partitioning technology, equivalence principle, and the boundary grid transformation technology. The distribution characteristics of ELF EMF in the two layers of polar seawater and sea ice are calculated, and the results clearly show the change of radiation intensity of ELF EMF in seawater. From these calculation results, it can be concluded that: At $d = 10$ m and $\rho = 125$ m from the interface between seawater and sea ice, the maximum radiation directions of EMF intensity are vertical electric field direction E_z and horizontal magnetic field direction H_x, respectively, and their average minimum attenuation rates in sea water medium are 30 dB and 20 dB, respectively, and their corresponding values in sea ice medium are 20 dB and 10 dB, respectively. Therefore, compared with other electric field and magnetic field directions, vertical electric field direction E_z and horizontal magnetic field direction H_x are more suitable for receiving low-frequency underwater signals. In addition, we compared the calculation results of the proposed method with those of Pan's approximate SNIM. The calculated results are consistent, and the average error was less than 5%, which meets the engineering requirements, thus verifying the accuracy and effectiveness of the proposed method.

REFERENCES

[1] H. Rowe, "Extremely low frequency communication to submarines," *IEEE Trans. Commun.*, vol. COM-22, no. 4, pp. 371–386, Apr. 1974.

[2] M. A. Yusof and S. Kabir, "An overview of sonar and electromagnetic waves for underwater communication," *IETE Tech. Rev.*, vol. 29, no. 4, p. 307, 2012.
[3] J. Macnae, "Stripping very low frequency communication signals with minimum shift keying encoding from streamed time-domain electromagnetic data," *Geophysics*, vol. 80, no. 6, pp. E343–E353, Nov. 2015.
[4] A. N. Sommerfeld, "Propagation of waves in wireless telegraphy," *Ann. Phys.*, vol. 333, no. 4, pp. 665–736, 1909.
[5] H. R. Zeng, T. He, L. Li, and K. Li, "Current distribution and input impedance of a horizontal linear antenna in the presence of a layered region," *IEEE Access*, vol. 7, pp. 84033–84039, 2019.
[6] L. He, T. He, and K. Li, "Quasi-static solution for ELF/SLF near-zone field of a vertical magnetic dipole near the surface of a lossy half-space," *Int. J. Antennas Propag.*, vol. 2020, pp. 1–13, Mar. 2020.
[7] J. Wang and B. Li, "Electromagnetic fields generated above a shallow sea by a submerged horizontal electric dipole," *IEEE Trans. Antennas Propag.*, vol. 65, no. 5, pp. 2707–2712, May 2017.
[8] H. L. Xu, T. T. Gu, and K. Li, "Approximated solutions for ELF near-field propagation due to a horizontal electric dipole excitation near the sea-rock boundary," *IEEE Trans. Antennas Propag.*, vol. 66, no. 5, pp. 2471–2481, May 2018.
[9] S. Hu, H. Xie, and T. Ding, "Electromagnetic field variation of ELF near-region excited by HED in a homogeneous half-space model," *Appl. Sci.*, vol. 13, no. 13, p. 7499, Jun. 2023.
[10] J. P. Berenger, "Finite-difference computation of VLF-LF propagation in the earth-ionosphere waveguide," in *Proc. EUROEM Symp.*, Bordeaux, France, Jun. 1994, vol. 6, no. 4, pp. 1734–1741.
[11] J.-P. Bérenger, "Reduction of the angular dispersion of the FDTD method in the earth-ionosphere waveguide," *J. Electromagn. Waves Appl.*, vol. 17, no. 8, pp. 1225–1235, Jan. 2003.
[12] J.-P. Berenger, "Long range propagation of lightning pulses using the FDTD method," *IEEE Trans. Electromagn. Compat.*, vol. 47, no. 4, pp. 1008–1012, Nov. 2005.
[13] Y. Xia and D. M. Sullivan, "Underwater FDTD simulation at extremely low frequencies," *IEEE Antennas Wireless Propag. Lett.*, vol. 7, pp. 661–664, 2008.
[14] C. M. Furse, "Faster than Fourier: Ultra-efficient time-to-frequency-domain conversions for FDTD simulations," *IEEE Antennas Propag. Mag.*, vol. 42, no. 6, pp. 24–34, Dec. 2000.
[15] K. Zheng, H. Luo, H. Yu, and J. Li, "A novel 3-D TSS-FDTD for distinguishing underwater targets at low frequency," *IEEE Antennas Wireless Propag. Lett.*, vol. 14, pp. 1814–1818, 2015.
[16] K. Zheng, H. Luo, Z. Mu, J. Li, and G. Wei, "Parallel TSS-FDTD method for analyzing underwater low-frequency electromagnetic propagation," *IEEE Antennas Wireless Propag. Lett.*, vol. 15, pp. 1217–1220, 2016.
[17] M. Yang, H. Peng, K. Zheng, and G. Wei, "Spatial radiation field distribution of underwater VLF two-element antenna array," *IEEE Trans. Antennas Propag.*, vol. 71, no. 1, pp. 1164–1169, Jan. 2023.
[18] W. Y. Pan, *LF VLF ELF Wave Propagation*. Chengdu, China: The Univ. Electron. Sci. Technol. Press, 2014, pp. 466–491.
[19] S. Shikhantsov, A. Thielens, G. Vermeeren, E. Tanghe, P. Demeester, L. Martens, G. Torfs, and W. Joseph, "Hybrid ray-tracing/FDTD method for human exposure evaluation of a massive MIMO technology in an industrial indoor environment," *IEEE Access*, vol. 7, pp. 21020–21031, 2019.
[20] T. Otim, A. Bahillo, L. E. Díez, P. Lopez-Iturri, and F. Falcone, "FDTD and empirical exploration of human body and UWB radiation interaction on TOF ranging," *IEEE Antennas Wireless Propag. Lett.*, vol. 18, no. 6, pp. 1119–1123, Jun. 2019.
[21] S. Burns, F. Gasdia, J. J. Simpson, and R. A. Marshall, "3-D FDTD modeling of long-distance VLF propagation in the earth-ionosphere waveguide," *IEEE Trans. Antennas Propag.*, vol. 69, no. 11, pp. 7743–7752, Nov. 2021.
[22] J. A. Roden and S. D. Gedney, "Convolution PML (CPML): An efficient FDTD implementation of the CFS-PML for arbitrary media," *Microw. Opt. Technol. Lett.*, vol. 27, no. 5, pp. 334–339, Dec. 2000.
[23] M. Abalenkovs, F. Costen, J.-P. Berenger, R. Himeno, H. Yokota, and M. Fujii, "Huygens subgridding for 3-D frequency-dependent finite-difference time-domain method," *IEEE Trans. Antennas Propag.*, vol. 60, no. 9, pp. 4336–4344, Sep. 2012.
[24] P. Pacheco, *Parallel Programming With MPI*. San Francisco, CA, USA: Morgan Kaufman, 1997.
[25] J. G. Van Blade, "High- and low-frequency fields," in *Electromagnetic Fields*, Z. Chen, Y. J. He, and L. Q. Gui, Eds., 2nd ed. Beijing, China: Tsinghua Univ. Press, 2013, pp. 671–732.

SUMOU HU was born in Jiujiang, China, in 1990. He received the B.S. degree in electronic science and technology from the People's Liberation Army University of Science and Technology, Nanjing, China, in 2016. He is currently pursuing the M.S. degree in information and communication engineering with the Naval University of Engineering, Wuhan, China. His current research interests include antennas, low-frequency electromagnetic wave propagation, and signal processing.

HUI XIE was born in Honghu, China, in 1978. He received the B.S. and M.S. degrees in information and communication engineering and the Ph.D. degree in information and communication engineering from the Naval University of Engineering, Wuhan, Hubei, China, in 2000, 2003, and 2007, respectively.

From 2007 to 2014, he was a Lecturer with the Naval University of Engineering. Since 2014, he has been an Assistant Professor with the Electronic Engineering Department, Naval University of Engineering. His research interests include low frequency antenna theory, electromagnetic field, and electromagnetic wave propagation.

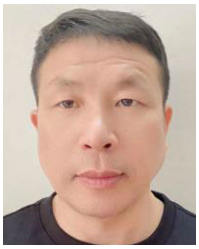

JIANCHEN FENG was born in Huanggang, China, in 1971. He received the B.S. degree in applied geophysics from Jilin University, Jilin, China, in 1995, and the M.S. degree in management science and engineering from the Harbin Institute of Technology, Heilongjiang, China, in 2010.

Since 2008, he has been a Senior Engineer with the Unit 91388 of the People's Liberation Army, Zhanjiang, Guangdong, China. His current research interests include weapons technology and equipment testing.